Morphology of graphite surfaces after ion-beam erosion

S. Habenicht
II. Physikalisches Institut and Sonderforschungsbereich 345, Georg-August-Universität Göttingen, Bunsenstrasse 7-9, D-37073 Göttingen, Germany

(Received 21 March 2000; revised manuscript received 30 October 2000; published 13 March 2001)

A review of the topographic evolution of (0001) highly oriented pyrolytic graphite surfaces eroded by 2–50 keV ion beams and investigated using scanning tunneling microscopy is given. For tilted incidence of the ion beam and intermediate ion fluences of about 10^{17} cm^{-2}, a periodic ripple topography with characteristic wavelengths between 40 and 700 nm was found. This morphology evolution is explained by a linear continuum theory of the interplay between material removal during sputtering and surface diffusion. The evolution of the surface morphology was measured as a function of the ion mass, the ion energy, and the target temperature. The validity of the linear erosion theory in the observed parameter space has been tested and its limitations for increasing fluences and ion energies and varying temperatures shown.

DOI: 10.1103/PhysRevB.63.125419 PACS number(s): 68.35.Bs, 79.20.Rf, 61.80.Jh

I. INTRODUCTION

Heavy ion irradiation is among the most prominent and versatile methods for surface and near-surface modification of solid materials. With the development of high-resolution observation techniques such as transmission and scanning electron microscopy (TEM, SEM),[1] field ion microscopy (FIM), and scanning tunneling and atomic force microscopy (STM, AFM),[2,3] it has become possible to investigate the effects of collision cascades, point defects, and defect aggregates in solids on the microscopic scale down to atomic resolution.

Since the development of these observation techniques, the evolution of surface morphology during ion bombardment has been the subject of intensive studies and controversial discussions. While for high ion energies ($E > 1-10$ MeV) plastic deformation and viscous flow of the surface material due to the electronic energy loss of the ions is accepted as the main physical agent of changes in the height topography,[4] for energies below these values different effects have to be taken into account. Among the most prominent features are radiation-induced diffusion,[5] selective grain growth,[6,7] and, especially for energies in the regime of nuclear stopping, ion-beam erosion due to sputtering of the surface material.[8] A review of various studies of the surface morphology during ion-beam erosion of graphite[9–11] will be given below. Finally, results on ion-beam erosion will be presented, in which the limitations of linear erosion theories will be shown.

The evolution of solid surface topography during ion-beam sputtering is governed by the interplay and competition between the dynamics of surface roughening on the one hand and material transport during surface diffusion on the other.[12,13] This competition is responsible for the creation of characteristic surface patterns such as self-affine topographies[14,15] and periodic ripples[16–21] when the ion beam is tilted to the surface normal. In Sec. II the theoretical background of these processes according to the theory of Bradley and Harper[22] will be presented briefly. The experimental recommendations for a detailed examination of these topics will be discussed in Sec. III. Then experimental results on ion beam erosion will be presented. Results gathered using the linear theory of Bradley and Harper will be tested in Sec. IV and finally their limitations will be shown in Sec. V. The entirety of these efforts will give an overview of the evolution of surface morphology during ion-beam erosion, and hopefully it will stimulate and give suggestions for further activities in this field of physics.

II. THE THEORETICAL BACKGROUND OF ION-BEAM EROSION

When an ion beam hits a solid surface, the kinetic energy of the projectiles dissipates into the material via kinematic collisions (the so-called nuclear energy deposition), by eletronic exitations (the so-called electronic energy deposition), and via thermal energy dissipation. Among these effects nuclear energy deposition is the dominating mechanism of material modification for the low- and medium-ion-energy regime studied in this work.

According to Sigmund's theory of nuclear energy deposition,[23,24] ion-beam sputtering is caused by recoil atoms within the collision cascade of the primary ion reaching sufficient energy to overcome the surface barrier. The sputtering yield Y, i.e., the number of sputtered atoms per incident ion, is defined to be proportional to the total amount of energy deposited on the surface $F_D(E,\theta,0)$. The distribution of the deposited energy $F_D(E,\theta,\mathbf{r})$ in the target material can be roughly described by the distribution of vacancies and recoils produced in the collision cascade in relation to the displacement energy E_D.[25] As the distribution of the deposited energy is proportional to the nuclear stopping power, it can be described in first order by a Gaussian distribution:

$$F_D(\mathbf{r}) = \frac{c}{(2\pi)^{3/2}\alpha\beta^2}\exp\left(-\frac{(z-h_0+a)^2}{2\alpha^2}-\frac{x^2+y^2}{2\beta^2}\right). \tag{1}$$

The accuracy of this approximation depends on the ion energy and the kinematics between projectile and target atoms. Although significant differences are observed for extremely asymmetric mass ratios between the colliding particles, the

parameters describing the distribution (a, α, and β) can be used to characterize the shape of the energetic impact into the near-surface region. Following the theoretical concepts of Refs. 13, 22, 26, and 27 the surface height evolution $h(\mathbf{r},t)$ can be described as

$$\frac{\partial h}{\partial t} = -F_0 + C\frac{\partial h}{\partial x} + C_x\frac{\partial^2 h}{\partial x^2} + C_y\frac{\partial^2 h}{\partial y^2} + \Lambda_x\left(\frac{\partial h}{\partial x}\right)^2 + \Lambda_y\left(\frac{\partial h}{\partial x}\right)^2 - B\nabla^4 h + \eta. \tag{2}$$

F_0 defines the surface erosion rate of a flat surface at normal incidence ($F_0 = \Phi Y_0/n$), which is directly related to the sputtering yield Y_0 of a flat surface. $C\partial h/\partial x$ is a term related to the derivative of the sputtering yield with respect to the angle of incidence, $C_{x,y}\partial^2 h/\partial x^2$, y^2 describes the linear curvature dependence of the surface erosion with $C_{x,y} = (\Phi a Y_0/n)\Gamma_{x,y}$, $\Lambda_{x,y}(\partial h/\partial x,y)^2$ being the nonlinear supplementation, and $B\nabla^4 h$ is the surface diffusion according to Wolf and Villain and to Mullins.[28] η defines the noise terms corresponding to the implantation process.

At intermediate ion fluences, when local slopes of the surface are moderate (described as the linear regime), this theory predicts the evolution of quasiperiodic surface ripples with a ripple wavelength of

$$\lambda_{x,y} = 2\pi\sqrt{2B/C_{x,y}}. \tag{3}$$

The ripple orientation should be perpendicular to the beam direction (as the wave vector points in the x direction of the surface, these ripples are called x waves) for incidence angles less than a critical angle θ_c, and parallel (called y waves) to the beam direction for incidence angles close to grazing. The wavelength of the ripple morphology therefore depends on the ratio between the surface mobility and the curvature dependence of the sputtering yield. Besides the surface mobility (which will be discussed later), the ripple morphology is affected experimentally by the kinematics of the collision process, and especially the ion mass and energy, which are the main parameters describing $C_{x,y}$ through the distribution of the deposited energy. Therefore the observed ripple wavelength should rise with increasing depth of the deposited energy and thus with increasing ion energy. The scaling of this increase supplies information about the distribution of the deposited energy and its evolution with increasing projectile energy. The evolution of the surface roughness $w(t)$ and the roughening factor R_k can also be extracted:

$$w(t) \propto \exp(R_k t), \tag{4}$$

$$R_k = \frac{[(\Phi a/n)Y_0\Gamma_{x,y}]^2}{4B}, \quad k_{x,y}^2 = \frac{(\Phi a/n)Y_0\Gamma_{x,y}}{2B}.$$

$k_{x,y}$ is the wave vector of the ripple structure occurring on the surface ($k_{x,y} = 2\pi/\lambda_{x,y}$). If thermal diffusion is assumed to dominate the surface smoothing process (for a special description of this topic, see Ref. 29), the Einstein relation fits for describing the surface mobility B and the ripple wavelength $\lambda_{x,y}$ should follow the temperature dependence[22]

$$\lambda_{x,y} \propto T^{-1/2}\exp\left(-\frac{\Delta E}{2kT}\right), \tag{5}$$

with ΔE being the activation energy for surface diffusion.

This description is supported by the results of Monte Carlo simulations on ion-beam-eroded carbon surfaces by Koponen *et al.*,[30,31] which predict surface ripple morphologies with nanometer scales ($\lambda = 15$–40 nm) and the switching of the ripple orientation when the incidence angle is tilted. Of course, in general surface diffusion is not an isotropic phenomenon on a crystalline surface, and surface steps will play an important role in the behavior of the surface mobility.[32] In fact, due to its low critical dose for a morphization,[33] the effects of anisotropy on surface diffusion and Ehrlich-Schwoebel barriers on graphite surfaces can be neglected and hence the effects are comparable to the theory. Since all erosion experiments occur in the regime of sputter equilibrium the saturation fluence Φ_s in the near-surface region can be obtained using Hubler's formula[5]

$$\Phi_s = \frac{3an}{2Y}. \tag{6}$$

Ripple morphologies have been investigated using scanning electron and probe microscopy (SEM, STM, AFM).[16,18–21] These effects will be discussed together with the experimental results of this work and compared to the theoretical predictions of the continuum theory.

III. EXPERIMENT

For a detailed examination of the erosion process on surfaces during ion bombardment, several experimental parameters such as the angle of incidence, the ion flux, the implantation fluence, and the ion energy have to be controlled.[34–36] The experiments were performed using freshly cleaved highly oriented pyrolitic graphite (HOPG) surfaces with (0001) orientation. The samples were irradiated at temperatures between 300 and 500 K with Ar^+ and Xe^+ ions at energies between 2 and 50 keV. Three different accelerators were used at the university of Göttingen: for ion energies of 2–10 keV the low-energy ion implanter[37] IOSCHKA was utilized, while the implantations at higher energies were performed using the heavy ion accelerators ADONIS (Ref. 38) and IONAS.[39] For all the implantations the ion flux was kept constant (8–12 μA/cm^2) to achieve comparable implantation conditions with different accelerators. Implantation fluences between 5×10^{16} and 5×10^{18} cm^{-2} were chosen for the erosion experiments. Homogeneous implantation was achieved via two-dimensional electrostatic sweeping. After irradiation, the samples were investigated under ambient conditions, using a NanoscopeII STM (Digital Instruments) and mechanically prepared $Pt_{80}Ir_{20}$ tips to observe the evolution of the height profile $h(\mathbf{r})$. Different area sizes (side length = 50 nm–3.5 μm) of the surfaces were scanned with the STM to observe both small- and large-scale morphology effects in the surface evolution. Wavelengths occurring on the surface were determined with the help of a structure fac-

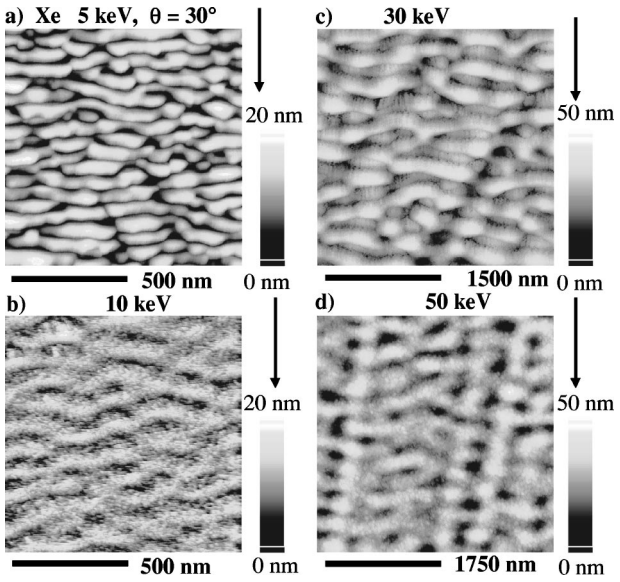

FIG. 1. STM micrographs (lateral size 1–3.5 μm) of 5–50 keV Xe^+-eroded HOPG surfaces. Irradiation fluence $\Phi=(3-5)\times10^{17}$ ions/cm^2; incident angle 30°. Ion energy (a) 5 keV, (b) 10 keV, (c) 30 keV, and 50 keV. Arrows indicate the ion-beam orientation.

tor calculation (for an explantation, see Ref. 9) and by direct examination of the surface periodicity.

IV. THE LINEAR REGIME

Recent work on the surface morphology of graphite during ion-beam erosion has shown a good agreement between experimental results and predictions of the linear erosion theory of Bradley and Harper. The ripple size, its orientation as a function of the incident angle and especially the change of its orientation as the angle rises above a critical value have been measured and compared to the theory as well as to Monte Carlo simulations of the erosion process (see Refs. 9, 11, 10, and 30). Furthermore evolution for high fluences leading to nonlinear behavior has been observed. Based on these experiences, additional investigations have been performed to examine the limitations of the model's validity, which will be presented in the following.

A. Energy dependence

Figure 1 shows STM micrographs of HOPG surfaces irradiated with Xe^+ ions at different ion energies between 5 and 50 keV. For these implantations, the angle of incidence was kept fixed at 30°. The same measurements were performed for Ar^+ ions. Ripple topographies are clearly visible in all the pictures, oriented perpendicular to the ion-beam projection onto the surface (the ion-beam projection has been inserted for each picture). The typical height differences between crests and valleys on the surface are between 10 and 20 nm, indicating that the sputtering yield (and therefore the deposited energy) is nearly constant in the energy range studied. The ripple spacing λ_x increases from 40 to 350 nm for Xe^+ and from 40 to 750 nm for Ar^+ ions. These observed

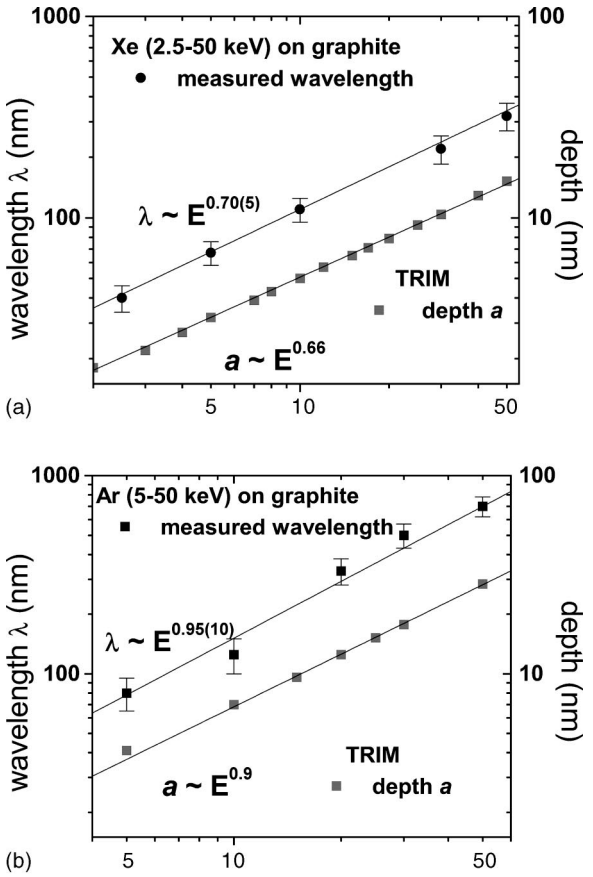

FIG. 2. Measured wavelengths λ as a function of the ion energy for Xe^+ ions (upper graph) and Ar^+ ions (lower graph). Power laws are fitted to both data sets. The dependency of the mean depth a of the deposited energy on the ion energy is added for both ions.

wavelengths correspond in magnitude to measurements on Si and SiO_2 reported previously.[18,19,21,29] Figure 2 presents the evolution of the ripple spacing as a function of the particle energy for both ions. The power laws $\lambda_x \propto E^p$ are fixed to the data, giving $p_{Xe}=0.70(5)$ and $p_{Ar}=0.95(10)$ for the exponents. There exponents agree with the evolution of the mean depth of the deposited energy with the ion energy as calculated with the deposited energy density F_D obtained from the stopping power[40] by Sigmund and co-workers.[23,41] This is a clear hint that the process is dominated by the nuclear stopping power. The difference between the exponents for the two ions is explained by the variation of kinematics between the projectile and the target atom.[5]

The evolution of the ripple wavelength $\lambda_{x,y}$ with ion energy E can be calculated analytically using Eq. (3) and the results of Bradley and Harper's theory[22] for $Y_0(\theta)$ and $\Gamma_{x,y}(\theta)$.[11,10] For a complete description of the shape of the damage cascade, both straggling parameters, longitudinal (α) and transverse (β) to the ion-beam direction, have to be taken into account. As a consequence λ_x increases linearly with a for this asymmetric mass ratio studied. Therefore power laws between λ_x and the energy, $\lambda_x(E)\propto E^p$ (as already mentioned) and between the depth a and energy, $a(E)\propto E^q$, with identical exponents $p(\mathrm{Ar,Xe})=q(\mathrm{Ar,Xe})$ should apply to both ions.

When comparing the experimental exponents $p(\mathrm{Xe}) = 0.70(5)$ and $p(\mathrm{Ar}) = 0.95(10)$ with the calculated values $[q(\mathrm{Xe}) = 0.66,\ q(\mathrm{Ar}) = 0.90]$, one finds excellent agreement for both ions. Consequently, for the energy range chosen and the very asymmetric mass ratio studied, depth and longitudinal straggling scale with the ion energy, while transverse straggling remains constant. However, this lateral spread of the damage cascade is mainly determined by the energy deposited into recoil cascades in the near-surface region. As the nuclear stopping power reaches its maximum and therefore just slightly varies in this regime (approx. 30% for Ar^+ and Xe^+ between 5 and 50 keV), the energy transfer into subcascades is nearly constant over a wide range. For rising ion energy, the near-spherical symmetry of the damage distribution at low energies (2 keV) develops into an ellipsoidal shape at $E = 50$ keV, while the damage track propagates into greater depths of the solid. Besides these conclusions, other effects, especially ion-induced diffusion[42,43] and relaxation,[18] are also discussed in the literature as affecting the ripple morphology as a function of the ion energy. The energy dependence of these effects, although they are supposed to be small compared to the cascade evolution, should be rather similar to the experimental results mentioned above. Therefore these effects cannot be excluded from the interpretation. They strengthen the dependence of the wavelength on the energy depth. Since both effects have been proposed in the sputtering theory, further experiments are needed to show which mechanism dominates the process of ion-beam erosion. In fact, the damage propagation into greater depths is reproduced by both theories.

V. LIMITATIONS OF THE LINEAR THEORY

A. Surface mobility during ion-beam treatment

In this section the role of the mobility of diffusing atoms on the surface during ion-beam treatment will be examined. If the surface diffusion is thermally activated, the surface mobility of the diffusing species is given by the Einstein relation. However, the energy deposition of the ion beam into the near surface region can affect several parameters of the surface mobility, such as the density of diffusing species, the surface free energy, and the activation energy for surface diffusion. As a consequence, an effect called radiation-enhanced diffusion (which should not be confused with the ion-induced diffusion mentioned in previous sections) is well known to be present in materials during ion bombardment.[5] Following the theory of Bradley and Harper,[22] the surface mobility can be estimated from the observed ripple wavelength and the measured surface roughness evolution as a function of the erosion time t, and the factor R_k can be extracted [see Eq. (4) and Fig. 3]. From this relation for 5 keV Xe^+ on graphite at room temperature a surface mobility of $1.3(3)\times 10^{-28}$ cm^4/s is obtained for these experimental conditions.

To observe the evolution of the surface mobility, measurements of ion-beam erosion at elevated target temperatures were performed. Figure 4 shows STM pictures of Xe-eroded surfaces at elevated temperatures, and Fig. 5 presents the evolution of the ripple spacing and of the surface roughness for 5 keV Xe^+-eroded graphite. Two effects can be observed: on the one hand, the wavelength of the surface ripples increases slowly with temperature, from 70 to 110 nm between 300 and 450 K, and, on the other hand, the surface roughness decreases with rising target temperature. Both effects are expected due to the increase of the surface mobility. Comparing the linear theory of ion-beam erosion with these values by approximating a thermally activated diffusion to the data [see Eq. (5)], one obtains an average activation energy of $E = 0.14(8)$ eV for both graphs, assuming thermally activated diffusion (for the limitations of this assumption, see Sec. II). This value is rather small compared to other activation energies for surface diffusion. It can be concluded that for this nonequilibrium process different mechanisms such as radiation-enhanced diffusion (RED) have to be taken into account. The energy deposited into the surface either affects the number of diffusing species or different diffusion paths are produced following the defect production during the ion bombardment.[5] In contrast to the mechanism of so-called ion-induced diffusion proposed by Makeev and Barabasi,[43] the effect of RED means a real material transport on the surface, which tends to smooth the surface roughness. As long as these radiation effects are superposed on the equilibrium mobility, conclusions concern-

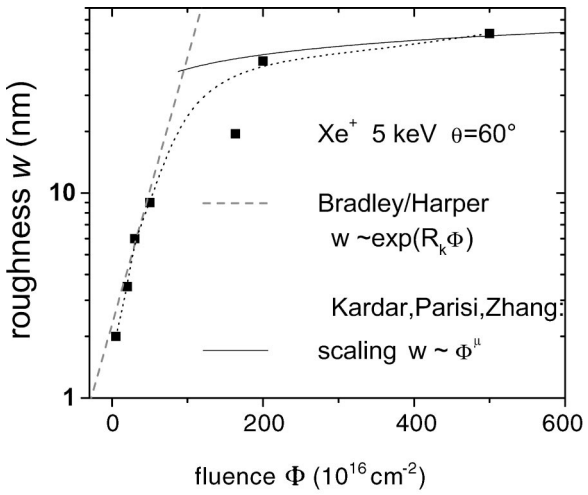

FIG. 3. Measured surface roughness as a function of the implantation fluence. The exponential growth can be explained by the linear theory. Above the transition a scaling regime is visible. The line is drawn to guide the eye.

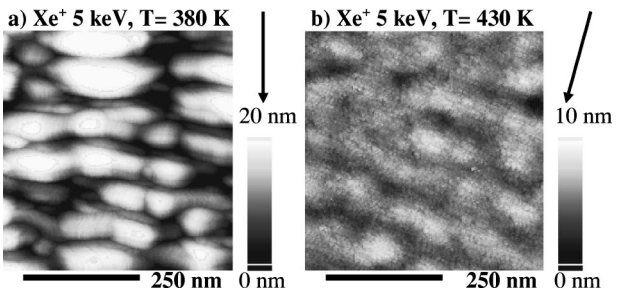

FIG. 4. STM micrographs (lateral size 0.5 μm) of 5 keV Xe^+-eroded HOPG surfaces at elevated temperatures.

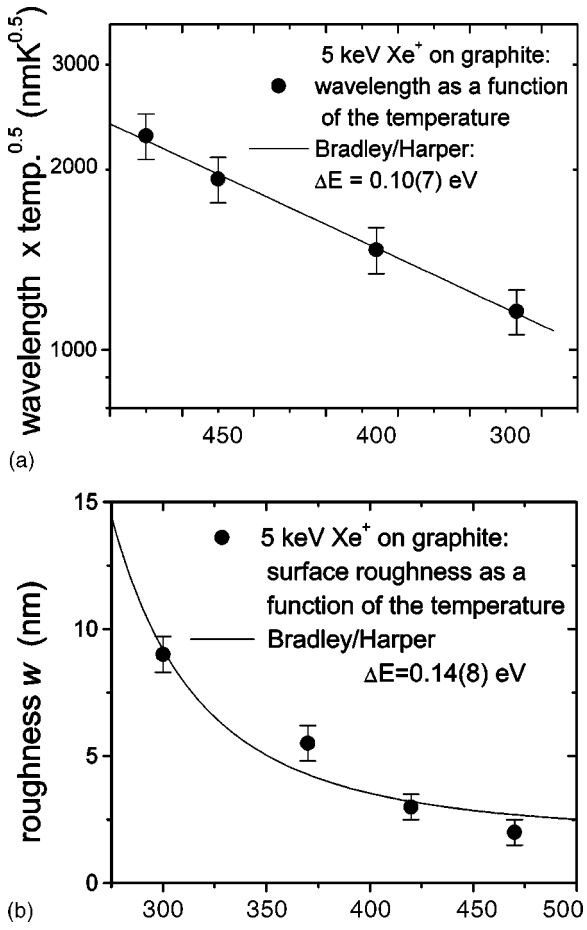

FIG. 5. Upper graph: measured wavelength as a function of the target temperature. Lower graph: measured surface roughness as a function of the target temperature. The approximations of the linear theory are added in both plots.

ing surface diffusion, beyond these general statements, are difficult to draw. Nevertheless, on other surfaces such experiments may be possible.[44]

B. Bulk effects for increasing ion energies

As long as ion-beam sputtering is the dominant process in morphology evolution, the effects of surface erosion mentioned above should dominate the mechanisms of surface roughening. In fact, this is the case for ion energies in the range of 1 up to 30–50 keV, depending on the kinematics between projectile and target atom, where nuclear energy loss and near surface damage are the major parameters describing the ion bombardment of solids. For increasing ion energy further implantation effects like bulk diffusion and other processes will become more and more important. The onset of this transition can already be seen in the graphite surfaces irradiated at 10–50 keV, where small-scale features and substructures on the ripple surface can be recognized. Figure 6 shows the evolution of these structures for increasing ion energy and increasing depth of deposited energy, using various ions. These features can be attributed to growth of impact nucleated segregations, referred to as grains, due to bulk diffusion induced by the ion beam. These

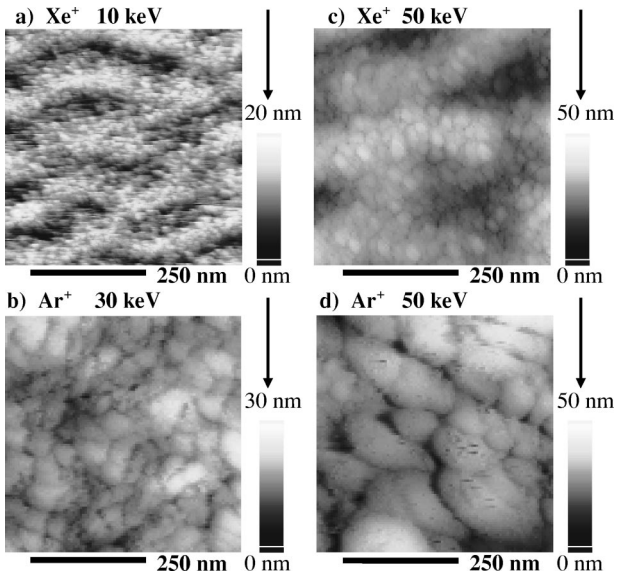

FIG. 6. STM micrographs of HOPG surfaces eroded at increasing energies. Small-scale features with increasing size are visible in all pictures, pointing to segregation and growth processes due to increasing saturation fluence.

radiation-enhanced diffusion processes were also suggested in Sec. V A to affect the temperature behavior of the ripple morphology. Although the microstructure of these segregations cannot be determined using STM, and a detailed examination is needed, the mechanism of nucleation and growth can be clearly identified. Small grains are nucleated by the deposition of energy and are successively ripened by further ion implantation. In this regime of fluence the grain size is not determined by the absolute ion fluence hitting the target—this can be seen in Fig. 1, where no grain growth effect is visible at 5 keV (see also Ref. 9)—but is governed by the saturation fluence Φ_s limited by the sputtering process in the near surface region. This saturation fluence increases for increasing ion energy (between 5 keV Xe and 50 keV Ar from ca. 5×10^{15} up to ca. 2×10^{17} cm^{-2}), because of the increasing depth of the deposited energy, which needs more time to become eroded after deposition. In this regime of fluence, nucleation and growth processes are known to have significant effects on surface and thin film morphologies. For rising saturation fluence this growth process starts to dominate the topography and finally completely covers the surface morphology evolution due to erosion. In Fig. 7 the average grain size l for each measurement is plotted against the critical fluence Φ_s for the implantation estimated with Eq. (6). The scaling law between grain size and saturation fluence ($l \propto \Phi_s^{0.7-1}$) suggests that a certain mechanism of nucleation and growth driven by ballistic collisions and defect formation at the grain boundaries and throughout the grains is involved in this process.[45,46] This conclusion is in agreement with the results mentioned in previous sections, where the process of energy deposition was characterized as dominated by the ballistic collisions of nuclear energy loss. This is known to be typical for the case of light target atoms.[25] With further experiments on this topic one will gain more

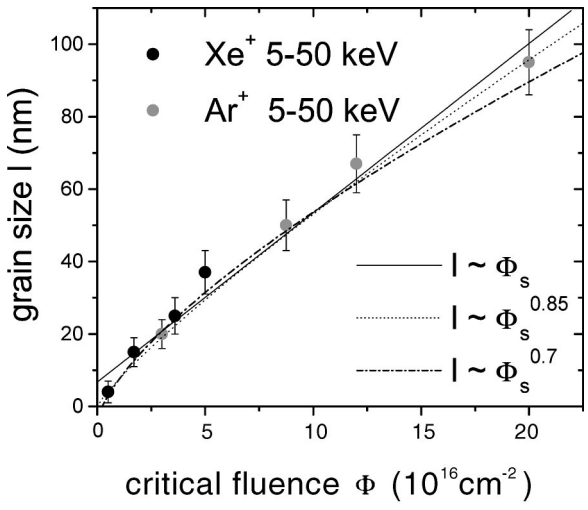

FIG. 7. Mean measured grain size l in the STM pictures plotted as a function of the saturation fluence Φ_s for the erosion experiments estimated with Eq. (8). Xe^+ and Ar^+ measurements are given separately.

insight into the grain microstructure and into details of the growth and diffusion processes.

VI. CONCLUSION AND OUTLOOK

In their entirety these experiments give an overview of morphology evolution on graphite after low-energy ion-beam sputtering. The linear theory of Bradley and Harper has been shown to describe the evolution of the surface topography in a wide range of parameters. These results show the ability of this model to predict and explain surface morphologies after ion-beam treatment and erosion as well as its limitations (beside the already known roughening transition at high ion fluences); on the one hand, to describe morphologies at high ion energy, where bulk processes start to dominate the topography, and on the other, to describe the surface mobility involved in these theoretical assumptions, if radiation-induced material transport on the surface has to be taken into account.

In any case, on increasing the ion energy two major changes in the surface treatment occur: electronic stopping and its effect on ion sputtering and damage production play a more and more important role in morphology evolution, and the maximum of the energy loss and therefore the damage production propagates for a greater depth into the material and mechanisms such as bulk diffusion and thermal spikes are superposed on the sputtering effects in the surface roughening.[6,7] Further efforts need to be made to gain deeper insights into these mechanisms. Electronic stopping is also known to have significant impact on collective and viscous relaxation phenomena, and it is the origin of viscous flow and shearing effects on solid surfaces under high-energy ion bombardment ($E>1$ MeV).[44] It would be of great interest to study all these effects in the surface topographic evolution of one material, while successively increasing the ion energy. From these insights conclusions can be drawn to define the region of dominant surface processes and a better understanding of the interplay of several surface and bulk effects like sputtering, thermal spikes, diffusion, and viscous relaxation is given.

ACKNOWLEDGMENTS

The author would like to thank Professor K. P. Lieb, Dr. U. Geyer, and Professor H. Hofsäss of Georg-August Universität Göttingen and Professor W. Bolse of Universität Stuttgart for their collaboration and discussions during this work. I. Koponen and M. Rost are acknowledged for their helpful discussions and suggestions. This work was funded by the Deutsche Forschungsgemeinschaft.

[1] H. Dammak, A. Dunlop, D. Lesueur, A. Brunelle, S. Della-Negra, and Y. Le Beyec, Phys. Rev. Lett. **74**, 1135 (1995).
[2] K. P. Reimann, W. Bolse, U. Geyer, and K. P. Lieb, Europhys. Lett. **30**, 463 (1995).
[3] W. Bolse, K. P. Reimann, U. Geyer, and K. P. Lieb, Nucl. Instrum. Methods Phys. Res. B **118**, 488 (1996).
[4] A. Gutzmann, S. Klaumünzer, and S. Meier, Phys. Rev. Lett. **74**, 2256 (1995).
[5] M. Nastasi, J. W. Mayer, and J. K. Hirvonen, *Ion-Solid Interactions, Fundamentals and Applications* (Cambridge University Press, Cambridge, 1996).
[6] A. Crespo-Sosa, P. Schaaf, W. Bolse, K. P. Lieb, M. Gimbel, U. Geyer, and C. Tosello, Phys. Rev. B **53**, 14 795 (1996).
[7] A. Rehmet and U. Geyer, Phys. Rev. B (to be published).
[8] P. Sigmund and G. Carter, in *Sputtering by Particle Bombardment I–III*, edited by R. Behrisch (Springer-Verlag, Heidelberg, 1983).
[9] S. Habenicht, W. Bolse, K. P. Lieb, K. Reimann, and U. Geyer, Phys. Rev. B **60**, R2200 (1999).
[10] S. Habenicht, K. P. Lieb, W. Bolse, U. Geyer, F. Roccaforte, and C. Ronning, Nucl. Instrum. Methods Phys. Res. B **161-163**, 962 (2000).
[11] S. Habenicht, W. Bolse, H. Feldermann, U. Geyer, H. Hofsäss, K. P. Lieb, and F. Roccaforte, Europhys. Lett. **50**, 209 (2000).
[12] C. A. Lang, C. F. Quate, and J. Nogami, Appl. Phys. Lett. **59**, 1696 (1991).
[13] A. L. Barabasi and H. E. Stanley, *Fractal Concepts of Surface Growth* (Cambridge University Press, Cambridge, 1995).
[14] E. A. Eklund, R. Bruinsma, J. Rudnick, and R. S. Williams, Phys. Rev. Lett. **67**, 1759 (1991).
[15] J. Krim, I. Heyvart, D. V. Haesendonck, and Y. Bruynserade, Phys. Rev. Lett. **70**, 57 (1993).
[16] E. Chason, T. M. Mayer, B. K. Kellerman, D. T. McIlroy, and A. J. Howard, Phys. Rev. Lett. **72**, 3040 (1994).
[17] G. Carter, M. J. Nobes, F. Paton, J. S. Williams, and J. L. Whitton, Radiat. Eff. **33**, 65 (1977).
[18] T. S. Mayer, E. Chason, and A. J. Howard, J. Appl. Phys. **76**, 1633 (1994).

[19] G. Carter, V. Vishniyakov, and M. J. Nobes, Nucl. Instrum. Methods Phys. Res. B **115**, 440 (1996).
[20] G. Carter and V. Vishnyakov, Phys. Rev. B **54**, 17 647 (1996).
[21] R. Schlatmann, J. D. Shindler, and J. Verhoeven, Phys. Rev. B **54**, 10 880 (1996).
[22] R. M. Bradley and J. M. E. Harper, J. Vac. Sci. Technol. A **6**, 2390 (1988).
[23] P. Sigmund, Phys. Rev. **184**, 383 (1969); Rev. Roum. Phys. **17**, 823 (1972).
[24] P. Sigmund, J. Mater. Sci. **8**, 1545 (1973).
[25] W. Bolse, Mater. Sci. Eng., R. **12**, 53 (1994).
[26] R. Cuerno and A. L. Barabasi, Phys. Rev. Lett. **74**, 4746 (1995).
[27] M. Rost and J. Krug, Phys. Rev. Lett. **75**, 3894 (1995).
[28] D. E. Wolf and J. Villain, Europhys. Lett. **13**, 389 (1990); W. W. Mullins, J. Appl. Phys. **28**, 333 (1957).
[29] J. Erlebacher, M. J. Aziz, E. Chason, M. B. Sinclair, and J. A. Floro, Phys. Rev. Lett. **82**, 2330 (1999).
[30] I. Koponen, M. Hautala, and O. P. Sievänen, Phys. Rev. Lett. **78**, 2612 (1997).
[31] I. Koponen, M. Hautala, and O. P. Sievänen, Nucl. Instrum. Methods Phys. Res. B **129**, 349 (1997).
[32] S. Rusponi, G. Costantini, C. Boragno, and U. Valbusa, Phys. Rev. Lett. **81**, 2735 (1998).
[33] T. Venkatesan, B. S. Elman, G. Braunstein, M. S. Dresselhaus, and G. Dresselhaus, J. Appl. Phys. **56**, 3232 (1984).
[34] R. Cuerno, H. A. Makse, S. Tomassone, S. T. Harrington, and H. E. Stanley, Phys. Rev. Lett. **75**, 4464 (1995).
[35] S. Park, B. Kahng, H. Jeong, and A.-L. Barabasi, Phys. Rev. Lett. **83**, 3486 (1999).
[36] M. Kardar, G. Parisi, and Y. C. Zhang, Phys. Rev. Lett. **56**, 889 (1986).
[37] S. Habenicht, W. Bolse, and K. P. Lieb, Rev. Sci. Instrum. **69**, 2120 (1998).
[38] H. Hofsäss, H. Binder, T. Klumpp, and E. Recknagel, Diamond Relat. Mater. **3**, 137 (1993).
[39] M. Uhrmacher, K. Pampus, F. J. Bergmeister, D. Purschke, and K. P. Lieb, Nucl. Instrum. Methods Phys. Res. B **9**, 234 (1985).
[40] J. F. Ziegeler, J. P. Biersack, and K. Littmark, *The Stopping and Ranges of Ions in Solids* (Pergamon, New York, 1985).
[41] K. B. Winterbon, P. Sigmund, and J. B. Sanders, Mat. Fys. Medd. K. Dan. Vidensk. Selsk. **37 (14)**, 1 (1970).
[42] S. W. MacLaren, J. E. Baker, N. L. Finnegan, and C. M. Loxton, J. Vac. Sci. Technol. A **10**, 468 (1992).
[43] M. A. Makeev and A. L. Barabasi, Appl. Phys. Lett. **71**, 2800 (1997).
[44] J. Erlebacher, M. J. Aziz, E. Chason, M. B. Sinclair, and J. R. Floro, J. Vac. Sci. Technol. A **18**, 115 (2000).
[45] H. A. Atwater, C. V. Thompson, and H. I. Smith, Phys. Rev. Lett. **60**, 112 (1988).
[46] J. Krug and H. Spohn, in *Solids Far from Equilibrium*, edited by C. Godreche (Cambridge University Press, Cambridge, 1991).